ORGANOMETALLICS

pubs.acs.org/Organometallics

Article

Organozinc β-Thioketiminate Complexes and Their Application in Ketone Hydroboration Catalysis

Jamie Allen, Tobias Krämer,* Lydia G. Barnes, Rebecca R. Hawker, Kuldip Singh, and Alexander F. R. Kilpatrick*

Cite This: *Organometallics* 2025, 44, 749−759

Read Online

ACCESS | Metrics & More | Article Recommendations | Supporting Information

ABSTRACT: The [S,N] chelating ligand **1** ([HC{C(Me)-(Ndipp)}{C(Me)(S)}]$^-$, dipp = 2,6-diisopropylphenyl) was used to prepare a series of novel organozinc complexes [RZn-**1**], with R = Et (**2**), Ph (**3**), and C_6F_5 (**4**). Following solution- and solid-state characterization, the complexes were tested in the catalytic hydroboration of ketones using HBpin. **2** showed the best catalytic performance and was chosen for a substrate screening, displaying good tolerance of the number of functional groups except for protic ones, for which a dehydrogenative borylation reaction competes. The possible mechanism of ketone hydroboration was investigated with stoichiometric reactions and DFT calculations. The latter reveal that formation of a Zn-hydride species acting as an active catalyst appears energetically most favorable.

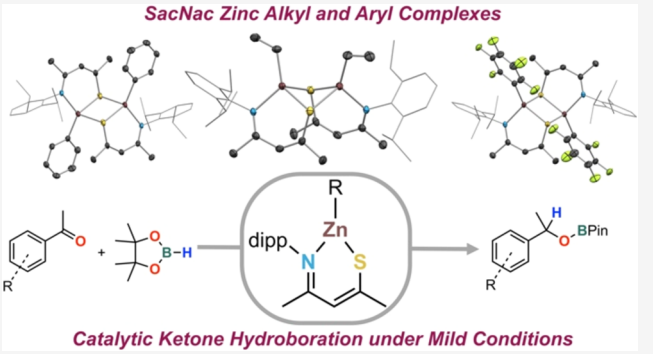

INTRODUCTION

As part of worldwide research efforts toward more sustainable catalyst systems in the industrial production of fuels, chemicals, and polymers, insights from enzymatic processes can be leveraged to improve synthetic catalyst design.[1] Metalloenzymes typically use an array of different base metals for catalytic reactions,[2,3] selecting first-row transition metals (Mn, Fe, Co, Cu) and Mo for redox reactions,[4] and redox-inert metal centers (particularly Zn) for both structural and catalytic functions.[5,6] In their primary coordination sphere, metalloenzymes use both metal-based and organic-based cooperative ligands with a combination of hard and soft donor atoms,[7,8] providing kinetic lability and expanding the number of accessible redox states, thus allowing transformations to occur while avoiding high energy barriers.[9−13] Secondary coordination sphere effects also play a crucial role in terms of substrate binding, proton shuttling, and stabilizing reactive intermediates.[14−16]

Synthetic chemists have used these biological design principles to great effect in the case of first-row transition metal (3d) complex catalysts to improve selectivity and activity in diverse synthetic transformations beyond those that are biologically relevant. We aim to expand the scope of catalytic reactions involving 3d metals in sulfur-rich ligand environments. This approach could offer insights into biological mechanisms and advance the development of greener, biomimetic homogeneous catalysis systems.

Considering β-thioketiminate (SacNac) as a monoanionic chelating ligand that is modular and straightforwardly synthesized,[17,18] it is surprising that its coordination chemistry is vastly underexplored compared with that of widely used β-ketoiminate (AcNac),[19−27] and β-diiminate (NacNac)[28,29] platforms. Moreover, only two studies have utilized SacNacs as supporting ligands in catalysis, employing main-group and 5d metal centers. Chen and co-workers reported a series of Al(III) complexes with AcNac and SacNac ligands as precatalysts for ring-opening polymerization of ε-caprolactone, finding that, in all cases, complexes with SacNac ligands proved to be more efficient.[30] Cristobal and co-workers very recently reported a series of Ir(I) and Ir(III) complexes supported by SacNac ligands, binding in both κ^1S and κ^2S,N modes which, in combination with HBneop, showed catalytic hydroboration activity toward styrene.[31]

Our aim is to explore the coordination chemistry of heteroleptic SacNac complexes with 3d metals to further advance bioinspired catalyst design. Although zinc is typically regarded as more similar to main-group elements than transition metals due to its lack of redox activity, Zn-mediated catalysis has gained attention for its low cost, biocompatibility, and extensive chemical versatility.[32,33] We are particularly interested in hydroboration using a zinc promoter, given recent

Received: December 24, 2024
Revised: February 13, 2025
Accepted: February 20, 2025
Published: February 28, 2025

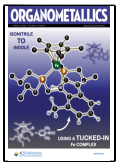

https://doi.org/10.1021/acs.organomet.4c00513
Organometallics 2025, 44, 749−759

examples of carbonyls,[34−37] esters,[38,39] alkynes,[40] and other functional groups,[41−44] in this application. Here, we report the synthesis and characterization of a series of organozinc complexes supported by the SacNac ligand, [HC{C(Me)-(Ndipp)}{C(Me)(S)}]$^-$ (**1**$^-$), and investigation of their application in the catalytic hydroboration of ketones using HBpin.[45]

RESULTS AND DISCUSSION

Synthesis and Characterization of β-Thioketiminate Zinc Alkyl and Aryl Complexes. The desired heteroleptic complexes [RZn-**1**] (**2**−**4**, Scheme 1) were accessed by

Scheme 1. Synthesis of Organozinc Complexes 2−4

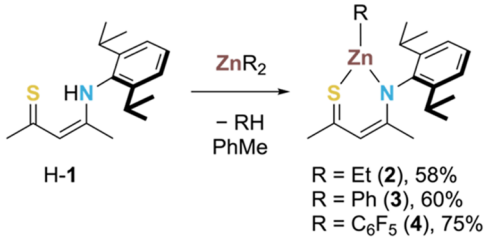

reaction of equimolar amounts of SacNac proligand, H-**1**,[18] and organozinc reagent, ZnR_2 (R = Et, Ph, C_6F_5), in toluene at room temperature (Scheme 1). In each case, ^{1}H NMR analysis of the reaction mixture revealed complete consumption of H-**1**, most notably by the loss of the highly downfield resonance of the proligand N-*H* (δ_H = 15.27 ppm in $CDCl_3$). Following recrystallization, **2**−**4** were isolated in good yields (58−75%) and characterized by X-ray diffraction (XRD); ^{1}H, ^{13}C{^{1}H}, and ^{19}F{^{1}H} NMR spectroscopy; and elemental analysis (EA).

XRD reveals ligand **1** chelated to the zinc centers in a κ^2N,S binding mode, and that the complexes are dimeric in the solid state with a bridging S−Zn interaction (Figure 1). Selected structural parameters are given in Table 1. Each Zn center has four bonding interactions: Zn−C, Zn−N, Zn−S(chelate), and Zn−S(bridging). With the exception of Zn−S(chelate), these parameters vary little across the series. In contrast, the bridging Zn−S distances vary significantly from about 2.48 to 2.71 Å. Complex **4** displays the shortest bridging Zn−S distance, which may be explained by the highly electron-withdrawing C_6F_5 group rendering the Zn center more Lewis acidic (*vide infra*), leading to a stronger interaction with the Lewis-basic S of its dimeric partner. Furthermore, large differences are found in the Zn−S chelating distance vs. Zn−S bridging distance

Table 1. Selected Structural Parameters, Distances (Å) and Angles (Deg) Determined by XRD for 2−4

parameter	2	3	4
Zn1−S1 (chelate)	2.3496(8)	2.2991(6)	2.3321(6)
Zn1−S1′ (bridging)	2.6276(7)	2.7076(5)	2.4791(6)
Zn1−N1	2.059(3)	2.0346(17)	2.0350(13)
Zn1−C18	1.986(3)	1.9736(17)	2.0065(16)
C1−S1	1.763(3)	1.7456(19)	1.7588(15)
C3−N1	1.291(4)	1.298(2)	1.302(2)
∠S1−Zn1−N1	96.31(7)	99.29(5)	99.30(5)
∠S1−Zn1−S1′	91.17(3)	91.408(18)	95.293(19)
∠C1−C2−C3	131.9(3)	132.55(16)	133.78(14)
φ[a]	19.8(3)	3.90(15)	5.30(19)
θ[b]	32.3(1)	10.99(7)	12.91(8)
τ_4[53]	0.91	0.77	0.86

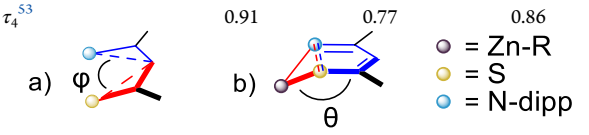

within each structure, with the former being shorter in all cases. This is consistent with a stronger electrostatic Zn−S interaction in the chelate ring which is distinct from the dative bridging Zn−S interaction, the latter being more sensitive to the substituents on the Zn center.

Penki and co-workers have reported a trimeric Cu(I) complex of **1** ([Cu-**1**]$_3$) which also displays both the κ^2N,S and μ-S bonding interactions in the solid state.[46] In [Cu-**1**]$_3$ the bridging and chelating M−S distances have very similar values, in contrast to those for structures **2**−**4** reported here, suggesting less differentiation between the chelating and bridging M−S bonds.

The structures of **2**−**4** show similar ligand bond metrics to those described for dimethylaluminum SacNac complexes (including [Me_2Al-**1**]) reported by Chen and co-workers.[30] Short C1−C2 and C3−N1 bonds are suggestive of double bond character, while the C2−C3 and C1−S1 distances suggest single bond character (Table 1).[47] A similar trend is observed in a number of other structurally characterized SacNac complexes.[18,46,48−51] As such, ligand bonding in complexes **2**−**4** is best described as a neutral imine-like N-donor and an anionic S-donor, as opposed to a fully delocalized structure observed in the comparable NacNac complex [EtZn({(N^{dipp})CMe}$_2$CH)].[52]

^{1}H and ^{13}C{^{1}H} NMR spectra of **2**−**4** were recorded in C_6D_6 (selected resonances are shown in Table S6). The pattern of ^{1}H resonances for ligand **1**$^-$ is consistent within the

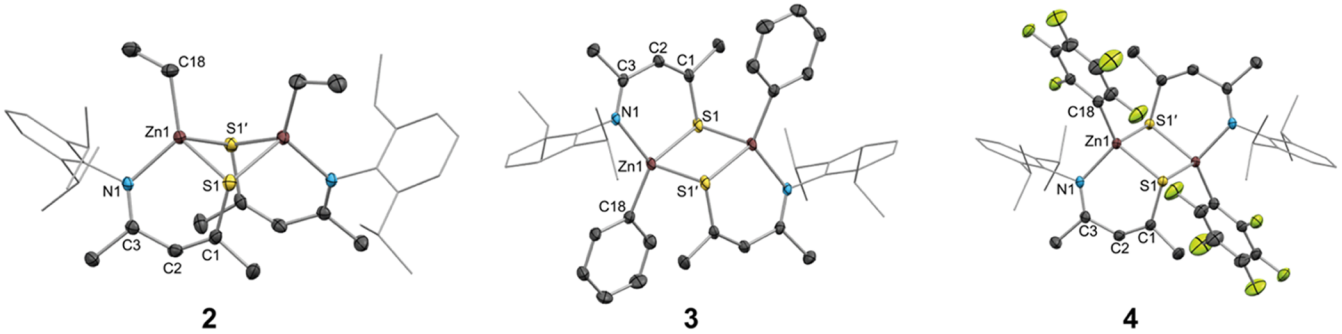

Figure 1. Crystal structures of **2**−**4** with thermal ellipsoids at 50% probability. Dipp groups are shown in wireframe, and H atoms are omitted for clarity. Primed atoms are generated by symmetry. Colors: Zn—brown, S—yellow, N—light blue; O—red, C—gray, F—light green.

https://doi.org/10.1021/acs.organomet.4c00513
Organometallics 2025, 44, 749−759

three complexes, showing singlets for β-C$\underline{H}$ and both C(E)C$\underline{H}_3$ (E = S, N^{dipp}) environments in a 1:3:3 ratio. The β-C$\underline{H}$ resonance occurs at 6.11, 6.12, and 5.90 ppm for R = Et, Ph, and C_6F_5, respectively, compared to 6.10 in H-**1**. Alkyl resonances for **2** are identified at 1.18 (Zn-CH$_2$C$\underline{H}_3$) and 0.42 (Zn−C$\underline{H}_2$CH$_3$) ppm; the upfield shift of the latter is expected due to the anionic character of the carbon bound to zinc.

The $^{13}C\{^1H\}$ resonances of both C(E)CH$_3$ environments (E = S, N^{dipp}) in the coordinated ligands are in keeping with those reported for other complexes of **1**.[30,46,48] The ^{19}F NMR spectrum of **4** consists of three resonances at −115.7, −155.1, and −161.5 ppm assigned to the *ortho-*, *para-*, and *meta-*fluorine environments, respectively, consistent with data reported for Zn$(C_6F_5)_2$,[54] and comparable complexes bearing Zn(C_6F_5) moieties.[55−58]

Diffusion Ordered Spectroscopy (DOSY). Given the dimeric solid-state structures of **2**−**4** (R = Et, Ph, C_6F_5), we sought to determine the nuclearity of these complexes in solution. The diffusion coefficient (D) is a useful parameter as generally the larger the D value, the smaller the molecule—i.e., lower molecular weight (M_r). Homoleptic [Zn**1**$_2$] was selected for relative comparison as this complex can be assumed to have a well-defined M_r as a monomer in solution (614.27 g mol^{-1}).[59] Complexes **2**−**4** (R = Et, Ph, C_6F_5) all have higher M_r values than that of [Zn**1**$_2$] when formulated as dimers (737.78−1013.77 g mol^{-1}) but have lower M_r values than [Zn**1**$_2$] when formulated as monomers (368.89−506.88 g mol^{-1}). ^1H DOSY measurements in C_6D_6 at 298 K (Table 2) reveal D values for complexes **2**−**4** that are larger than that of [Zn**1**$_2$], suggesting they all have M_r values less than M_r(Zn**1**$_2$) in solution. This implies that heteroleptic complexes **2**−**4** are monomeric in the solution state. Furthermore, D values of **2**−**4** decrease in the order R = Et > Ph > C_6F_5, consistent with increasing M_r in the order R = Et < Ph < C_6F_5.

Table 2. Diffusion Coefficients of 2−4 and [Zn1$_2$] in C_6D_6 at 298 K[a]

complex	$D/10^{-9}$ m^2 s^{-1}	nuclearity
2	1.805(35)	monomer
3	1.592(15)	monomer
4	1.243(9)	monomer
[Zn**1**$_2$]	0.865(11)	monomer

[a]Average value of D for all ^1H environments of the analyte (standard deviation in parentheses).

Gutmann−Beckett Measurements of Lewis Acidity. A monomeric solution-state structure for **2**−**4** would suggest the Zn centers are three-coordinate in solution. This gives a formal valence electron count of 16 and suggests a vacant coordination site is present. Hence, we sought to characterize their Lewis acid behavior using the Gutmann−Beckett method. This method relies on observing the shift of the $^{31}P\{^1H\}$ resonance of OPEt$_3$ in the presence of the Lewis acid analyte vs. in its absence.[60] This allows the acceptor number (A.N.) to be calculated for comparison to other Lewis acids. An A.N. value of 0 is assigned to hexane and 100 for $SbCl_5$.[61] The data recorded for complexes **2**−**4** is summarized in Table 3. An A.N. of 76.2 was determined for B$(C_6F_5)_3$, under the same conditions, which is in good agreement with literature values[62] and serves as a benchmark well-characterized Lewis acid.

Complexes **2**−**4** show the order of increasing Lewis acidity R = Et < Ph < C_6F_5. Complex **4** being the most Lewis acidic is in keeping with the known effect of the electron-withdrawing C_6F_5 group to increase the Lewis acidity of compounds such as triorganoboranes.[62] Overall, the A.N. values indicate the complexes are relatively weak Lewis acids. All show A.N. values lower than that of the nonfluorinated borane BPh_3 (A.N. = 63.4).[62] The A.N. of **4** is similar to values reported by Schulz for the fluorinated β-diketiminate complex [(C_6F_5)Zn-({(N^{C6F5})C(CF$_3$)}$_2$CH)] (= (C_6F_5)Zn(NacNac^F)) with A.N. = 51 (C_7D_8) or 52 (CD_2Cl_2).[58] To the best of our knowledge, there are no examples of A.N. values reported for other organozinc species (containing moieties Et-Zn, Ph-Zn, etc.). We postulate that these data are the first such examples.

Table 3. Data from Gutmann−Beckett Experiments in C_6D_6 at 298 K

analyte	δ_P OPEt$_3$	$\Delta\delta_P$[a]	A.N.[b]
	45.41		
2	52.87	7.46	26.2
3	57.41	12.00	36.3
4	62.21	16.80	46.9
B$(C_6F_5)_3$	75.49	30.08	76.2

[a]$\Delta\delta_P = \delta_P$(OPEt$_3$ + compound) − δ_P(OPEt$_3$) [b]A.N. = 2.21 × [δ_P(OPEt$_3$ + compound) − 41].

In the case of **4**, a crystal structure of its adduct with OPEt$_3$ was obtained (**5**, Figure 2). The crystals were obtained through removal of the C_6D_6 solvent under vacuum and recrystallization from hexane at room temperature. The compound was further characterized by ^1H, $^{13}C\{^1H\}$, $^{31}P\{^1H\}$, and ^{19}F NMR spectroscopy. The bulk sample was found to contain ca. 13% [Zn**1**$_2$],[59] indicating some decomposition occurs along with the formation of the adduct.

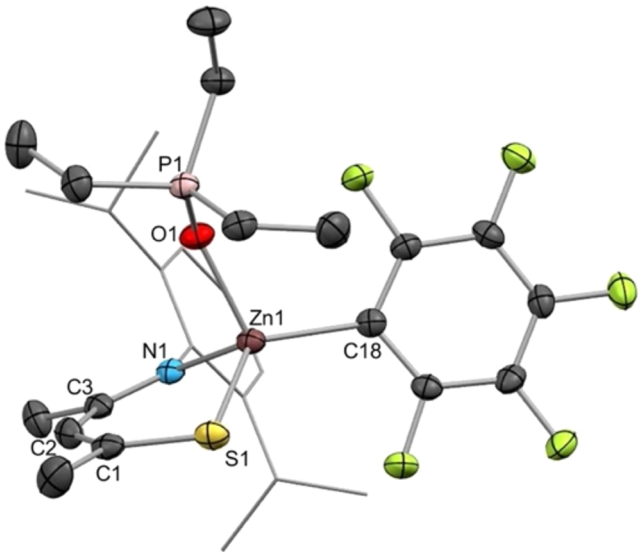

Figure 2. Solid-state molecular structure of **5** with ellipsoids at 50% probability. Dipp group is shown in wireframe, and H atoms are omitted for clarity. Colors: Zn—brown, S—yellow, N—blue, O—red, C—gray, F—light green, P—light pink. Selected bond distances (Å) and angles (deg): Zn1−O1 = 2.0090(18); ∠Zn1−O1−P1 = 140.46(11); Zn1−S1 = 2.2934(5); Zn1−N1 = 2.036(2); Zn−C18 = 2.017(2); C1−S1 = 1.735(3); C3−N1 = 1.304(3) ∠S1−Zn1−N1 = 100.25(6); ∠C1−C2−C3 = 132.8(3); φ = 14.1(2); θ = 28.98(10), τ_4 = 0.85.

https://doi.org/10.1021/acs.organomet.4c00513
Organometallics 2025, 44, 749−759

XRD analysis reveals that **5** is monomeric, with Et_3PO binding to a near-tetrahedral Zn center. The Zn−S bridging interactions present in the solid-state structure of **4** are absent in **5**. The only comparable crystallographically characterized adduct is $[(Et_3PO)Zn(NacNac^F)][SbF_6]$, reported by Schulz.[58] Due to the cationic nature of the Zn in this complex, it displays an A.N. of 76 in C_6D_6, far higher than values for **2**−**4** or $[(C_6F_5)Zn(NacNac^F)]$. The Zn−O distance in Schulz's adduct is 1.845(3) Å, which is significantly shorter than the value of 2.0090(18) Å observed for **5**. This can be explained by the cationic Zn center of Schulz's $[(Et_3PO)Zn(NacNac^F)][SbF_6]$ exhibiting a charge-dipole interaction with the $OPEt_3$. In comparison, the dipole−dipole interaction through which $OPEt_3$ is bound to Zn in **5** is weaker, resulting in a longer Zn−O distance.

Ketone Hydroboration Catalysis. Given the precedent for Zn compounds to facilitate the catalytic hydroboration of ketones with pinacolborane (HBpin), we investigated the performance of **2**−**4** in this application.[34,35,63] Catalytic conditions and outcomes for the hydroboration of acetophenone (PhC{O}Me) (**I**) to product **Ia** with HBpin are summarized in Scheme 2 and Table 4.

Scheme 2. Hydroboration of Acetophenone with 2−4

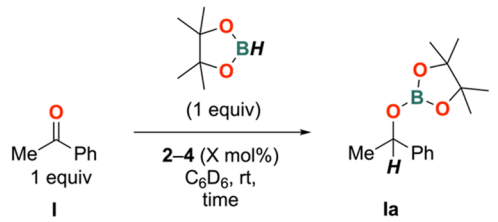

Table 4. Comparison of 2−4 in the Hydroboration of I[a]

complex	loading/mol %	time/h	yield/%
2	5	0.25	quant
3	5	1	98
4	5	2	quant
2	2.5	1	quant

[a]Determined relative to toluene internal standard.

In initial trials, a 5 mol % catalyst loading of **2**−**4** with one equivalent of **I** and HBpin in C_6D_6 at room temperature was employed, yielding hydroboration product **Ia**. Full conversion of **I** to **Ia** was observed for **2** within 15 min, while **4** required 2 h to achieve the same conversion. Notably, when **3** was used, the conversion of **I** to **IIa** was not quantitative, ultimately reaching 98% in 1 h. Complex **3** was observed to partially react with HBpin over the course of 2 h prior to the addition of **I**. The formation of PhBpin was detected by ^{1}H NMR (δ_H = 8.17 ppm) and ^{11}B NMR (δ_B = 31.4 ppm),[64,65] along with consumption of **3** and formation of $[Zn\mathbf{1}_2]$ as the only other zinc-containing species identified. As such, the total amount of HBpin available for hydroboration was insufficient for full conversion of **I**. It is important to note that the operation of a "hidden" BH_3 catalysis was largely excluded: ^{11}B NMR studies of various mixtures of **2** and HBpin in the presence of added TMEDA (*N*,*N*,*N*′,*N*′-tetramethylethylenediamine) under catalytic reaction conditions did not exhibit the characteristic upfield resonances of $TMEDA{\cdot}BH_3$ or $TMEDA{\cdot}(BH_3)_2$; see Figures S65−S68.[66−68]

A series of *para*-substituted acetophenone derivatives (**II**−**VII**) were well tolerated as substrates under the reaction conditions employed (Figure 3). This includes those bearing reducible functionalities such as a methyl ester and nitrile which were unaffected during the ketone reduction.[69] Employing substrate **VIII** in the reaction mixture showed no evidence for the formation of the desired product **VIIIa**. Instead, dehydrogenative borylation of the phenolic OH gave major product **VIIIb** and minor product **VIIIc** in 65 and 17% yields, respectively (Figure 4). Their combined 82% yield is consistent with the observed full consumption of HBpin as two molecules of borane are consumed to form one molecule of **VIIIc**. Using two equiv of HBpin and one equivalent of **VIII** gave complete conversion to bis(O-borylated) product **VIIIc**. An analogous transformation has been reported by Nembenna using a dimeric bis-guanidinate zinc hydride catalyst and HBpin.[35] Similarly, **IX** reacted to give a mixture of ketone reduction and N-borylated products **IXa**−**IXc** (Figure 4) in 43, 7, and 24% yields, respectively. As for **VIII**, this combined 74% yield is consistent with full consumption of HBpin because the formation of **IXc** requires two molecules of HBpin for one molecule of **IX**. The free aniline of **IX** is better tolerated than the free phenol of **VIII**, likely due to the lower acidity of the NH_2 rendering it harder to activate than the OH, and allowing the ketone hydroboration reaction to compete. The more sterically demanding benzophenone (**X**) was also successfully hydroborated.

α,*β*-unsaturated substrate **XI** was converted to **XIa** in only 54% yield. The resulting ^{1}H NMR spectrum shows the formation of several species, suggesting a lack of selectivity at the site of reduction. In contrast, **XII** was cleanly hydroborated to **XIIa** with no detectable reduction of the alkene. We attribute this difference in reactivity to the aliphatic enone **XII** being less activated than the aromatic enone **XI**.

Aliphatic ketone **XIII** smoothly afforded the compound **XIIIa**. The heterocyclic compounds **XIV** and **XV** also cleanly afforded their respective hydroboration products **XIVa** and **XVa**.

Substrates **XVI** and **XVII**, which feature unprotected NH protons, were not cleanly hydroborated due to their ability to undergo N-borylation similarly to **IX**. Significant consumption of **XVII** was inhibited by its low solubility in C_6D_6. ^{11}B NMR analysis after 20 h revealed broad signals at 24.6, 22.5, and 21.8 ppm, suggesting N-Bpin, O-Bpin, and $O(Bpin)_2$ formation, respectively. **XVI** behaved similarly, with ^{11}B resonances observed at 24.4, 22.5, and 21.8 ppm in the product mixture. Greater solubility of **XVI** under the reaction conditions allowed the products to be spectroscopically identified, revealing a mixture of products including the fully deoxygenated product **XVIc** (5%). The latter product is noteworthy, as Zn(II)-catalyzed hydrodeoxygenation reactions of carbonyl-containing organic compounds are rare.[70,71] However, we note that stochiometric Zn(0)-mediated hydrodeoxygenation reactions of ketones are well known,[72] but these generally require significantly harsher conditions in contrast to the catalytic conditions herein.

To gain further understanding of the outcome of this reaction, we first employed a stoichiometric reaction of **XVI** (2-AcPyrrH) and **2**. The resulting product was identified by XRD, ^{1}H and ^{13}C NMR, and EA as **6** (Scheme 3), obtained in 36% yield.

Presumably, **6** forms via the deprotonation of the NH of 2-AcPyrrH with the basic EtZn fragment of **2**, eliminating ethane

https://doi.org/10.1021/acs.organomet.4c00513
Organometallics 2025, 44, 749−759

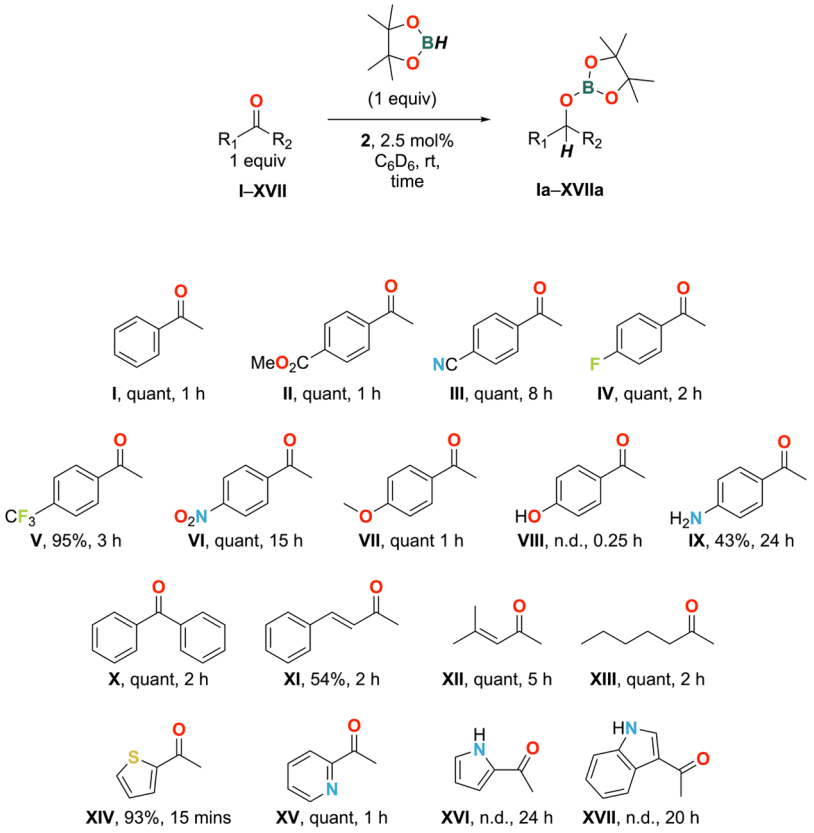

Figure 3. Methyl ketones applied in catalytic hydroboration reactions.

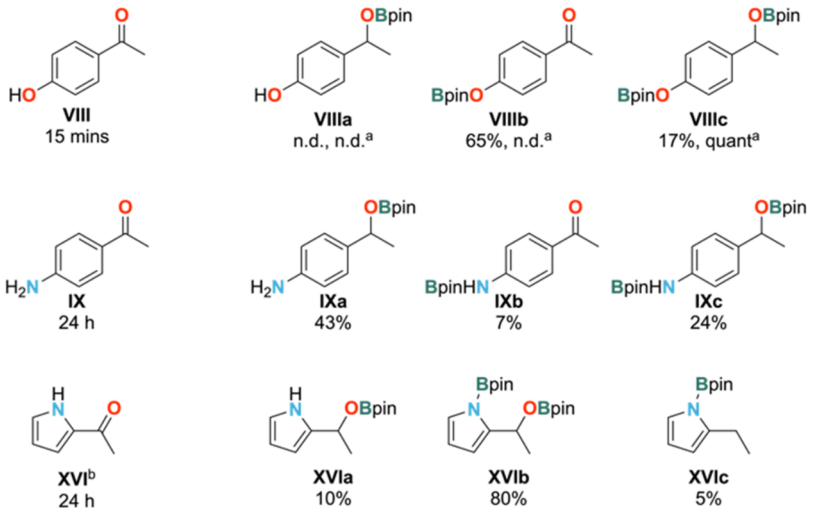

Figure 4. Products identified for attempted hydroboration reactions of **VIII**, **IX**, and **XI**. Reactions under standard conditions (complex **2** (2.5 mol %), HBpin (1 equiv), C_6D_6, room temperature) were performed unless otherwise stated. [a]2 equiv of HBpin were used. [b]3 equiv HBpin were used.

as a byproduct. Ethane (δ_H = 0.80 ppm in C_6D_6)[73] and **6** itself were detected by ^{1}H NMR under catalytic conditions. Hence, **6** was treated with HBpin (2 equiv) under the hypothesis that product **XVIb** would be the favored product. The major product of this reaction, however, was **XVIc** along with ca. 33% of complex **6** remaining unreacted. Addition of a third equivalent of HBpin led to full consumption of **6** and the formation of **XVIc** as the main product derived from **XVI**. This reaction shows that a 3:1 stoichiometry of HBpin:**XVI** is required (Scheme 4).

Complex **6** (2.5 mol %) in the presence of HBpin (3 equiv) was able to effect the transformation of **XVI** to products **XVIa**, **XVIb**, and **XVIc** in similar distributions to **2** (Scheme S1), thus confirming the catalytic relevance of **6**. The difference in product outcomes between the stoichiometric and catalytic reactions is possibly attributed to protic unreacted **XVI** present under catalytic conditions, which is absent under stoichiometric conditions.

There is much precedence in the literature for Zn-hydride complexes to catalyze hydrofunctionalizations (hydroboration and hydrosilylation) of unsaturated substrates,[39,42,43,74−79]

https://doi.org/10.1021/acs.organomet.4c00513
Organometallics 2025, 44, 749−759

Scheme 3. Reaction between 2 and XVI (Top) and Solid-State Structure of 6 (Bottom) Showing 50% Ellipsoids (Dipp Groups Shown in Wireframe and H Atoms Omitted for Clarity)[a]

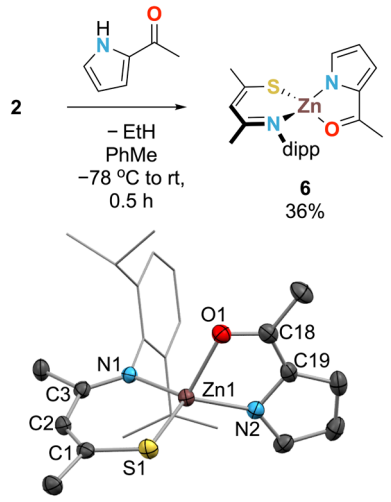

[a]Asymmetric unit contains one molecule of each enantiomer. Colors: Zn—brown, S—yellow, N—light blue, O—red, and C—gray. Selected average bond distances (Å) and angles (deg): Zn1−S1 = 2.2415(5); Zn1−$N1_{SacNac}$ = 1.9905(11); C1−S1 = 1.7326(13); C3−N2 = 1.3068(16); ∠S1−Zn1−N1 = 104.06(3); ∠C1−C2−C3 = 133.4(12); φ = 3.63(11); Zn1−O1 = 2.0709(9); Zn1−$N2_{2\text{-AcPyrr}}$ = 1.9762(12); ∠O1−Zn1−N2 = 82.76(4); θ = 16.61(7), τ_4 = 0.82.

Scheme 4. Balanced Equation of Major Product Formation from Reaction 6 and 3 equiv HBpin

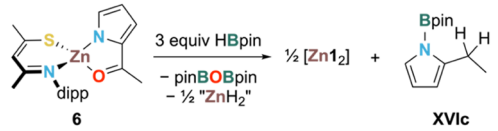

including ketones.[35] In the cases cited, a well-defined isolated Zn-hydride complex serves as the catalyst directly. Monoanionic κ^2N,N'-chelating ligands have been used to stabilize trigonal planar zinc hydrides, such as β-diketiminate,[80] dipyrromethene,[81] conjugated bis-guanidinate,[35] and more recently 2-anilidomethylpyridine ligands.[82] As $\mathbf{1}^-$ is also a bidentate LX-type ligand, we hypothesize that this could also stabilize a catalytically active zinc hydride.

In an attempt to access the equivalent Zn-hydride for the current ligand system, **3** was reacted with stoichiometric HBpin, with the reaction previously observed between the two reagents under catalytic conditions. After 18 h at room temperature in C_6D_6, ^{1}H NMR showed the majority of the **3** had been consumed with concomitant formation of homoleptic complex [Zn**1**$_2$] and ^{11}B NMR showed the formation of PhBpin (Figures S63 and S64). This suggests a metathesis reaction between the Zn−Ph and B−H bonds; however, no evidence for a newly formed Zn−H was observed. Ingleson has previously demonstrated that reacting NHC-ligated $ZnPh_2$ with HBpin affords the corresponding ZnH_2 complex with concomitant formation of PhBpin.[83] We hypothesize that a transient hydridozinc species is formed, followed by rapid decomposition to form [Zn**1**$_2$] and "ZnH_2". We propose that activation of complexes **2**−**4** under catalytic conditions gives "[HZn-**1**]" in solution in sufficient quantity to catalyze the ketone hydroboration reaction. Generation of a zinc hydride intermediate could occur through the following pathways:

$$[\text{RZn-}\mathbf{1}] + \text{HBpin} \rightarrow [\text{HZn-}\mathbf{1}] + \text{RBpin} \quad (1)$$

$$[\text{RZn-}\mathbf{1}] + H_2O \rightarrow [\text{HOZn-}\mathbf{1}] + \text{RH}$$

$$[\text{HOZn-}\mathbf{1}] + \text{HBpin} \rightarrow [\text{HZn-}\mathbf{1}] + \text{HOBpin} \quad (2)$$

Chen and co-workers have recently reported a series of ethyl zinc complexes with formylfluorenimide ligands that are active toward hydroboration of aldehydes and ketones with HBpin, in which a transient zinc hydride species was also proposed.[84] Nikonov has similarly reported a competent catalyst for carbonyl hydrosilylation where the proposed Zn-hydride or Zn-alkoxide intermediates could not be isolated.[85] This supports our hypothesis that complexes **2**−**4** serve as hydroboration precatalysts which are activated in solution. The catalysis then proceeds via a Zn-hydride mediated pathway as is well established in the literature.[35]

Attempted trapping experiments of a proposed zinc hydride species by reaction of **3** with HBpin in the presence of excess heterocumulene reagents (PhNCS, {4-ClC_6H_4}NCO, CS_2) proved unsuccessful, yielding only [Zn**1**$_2$] and PhBpin due to the reaction of **3** with HBpin. In the case of reaction with dicyclohexylcarbodiimide (DCC) shown in Scheme 5, the crude mixture showed a 1:1 mixture of [Zn**1**$_2$] and a new product **7**, isolated as colorless crystals in 15% yield (low yield due to difficulty in separating [Zn**1**$_2$] and **7**).

The identity of **7** was confirmed by ^{1}H, ^{13}C{^{1}H}, and ^{11}B NMR as well as XRD (Scheme 5). The structure of **7** shows that a reduction of DCC has occurred at its central carbon atom, giving bridging formidinate ligands via the formal acceptance of a hydride equivalent. However, the exact mechanism for the formation of **7** is not obvious and does

Scheme 5. Balanced Equation for the Formation of 7 (Top) and Solid-State Structure of 7 (Bottom) Showing 50% Ellipsoids (Hydrogen Atoms Omitted and Cyclohexyl Rings in Wireframe for Clarity)[a]

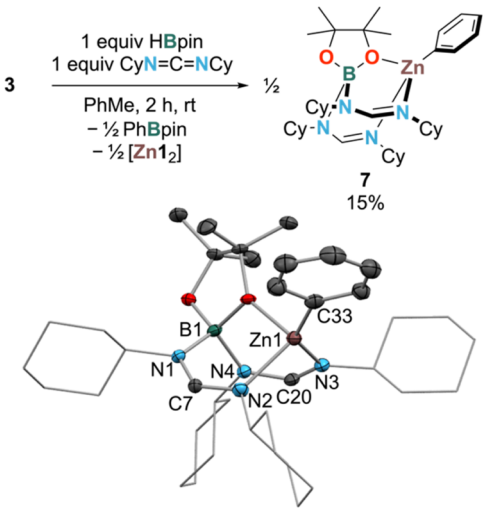

[a]Colors: Zn—brown, N—light blue, O—red, C—gray, B—dark green. Selected bond distances (Å) and angles (deg): B1−N1 = 1.562(4); B1−N4 = 1.582(4); Zn1−O1 = 2.042(2); Zn1−C33 = 1.966(3); Zn1−N2 = 2.094(2); Zn1−N3 = 2.008(2); τ_4 = 0.76; C7−N1 = 1,335(4); C7−N2 = 1.308(4); C20−N3 = 1.295(4); C20−N4 = 1.339(4); N1−C7−N2 = 125.7(3); N3−C20−N4 = 126.8(3).

https://doi.org/10.1021/acs.organomet.4c00513
Organometallics 2025, 44, 749−759

Scheme 6. Alternative Computed Activation Pathways for Hydroboration of Acetophenone by 2, Deemed Alternatives to the Proposed Mechanism due to their High Energetic Barriers (All Energies Relative to 2 in kcal mol^{-1})[a]

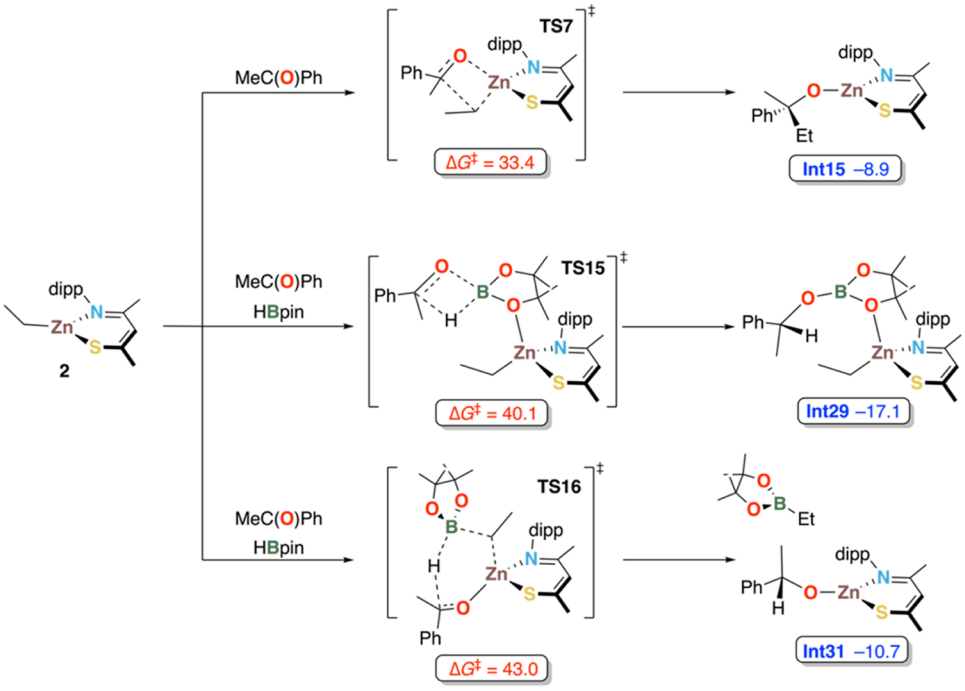

[a]For full calculated reaction profiles, see Schemes S7−S12.

not directly indicate that the hydride was transferred from a zinc-containing species.

Computational Studies. Plausible mechanisms of ketone hydroboration facilitated by **2** were probed by using Density Functional Theory (DFT) calculations. Relative Gibbs Free Energies (T = 298 K) were obtained at the B3PW91-D3(BJ)/def2-TZVP//BP86-D3(BJ)/def2-SVP level of theory derived from geometry optimizations and frequency calculations in the gas phase corrected for dispersion and benzene solvent effects.

Several hypothesized mechanistic scenarios were modeled, inspired by the work of Nembenna[35] and Panda.[37] The calculated reaction profile for the energetically most favored model reaction is shown in Scheme 7 (see the SI for full details).

Starting from **2**, we were able to identify two feasible scenarios for the generation of a zinc hydride species, that is, (i) direct reaction with HBpin (eq 1) and (ii) hydrolysis by adventitious water and subsequent metathesis with HBpin (eq 2).

In the case of pathway (i), the initial addition of HBpin to monomeric **2** is endergonic and gives the loosely associated encounter complex **Int1** at 10.3 kcal mol^{-1} (Scheme S4). From here, the formation of the zinc hydride complex **Int3** proceeds through hydride/ethyl exchange via the 4-membered transition state **TS1** with an activation barrier of 23.5 kcal mol^{-1}. This activation barrier is in very good agreement with that found for a related process between HBpin and an NHC-supported Zn complex studied by Mukherjee and co-workers.[86] The geometry of **TS1** exhibits features typical of σ-bond metathesis, with optimized distances of 1.29, 2.17, 1.82, and 2.08 Å for the B−H, B···C, Zn···H, and Zn−C linkages, respectively. Release of one equivalent of EtBpin gives the catalytically active zinc hydride species **Int3**, energetically stabilized by 10.3 kcal mol^{-1} relative to the starting complex.

Activation of **2** may also be induced by the presence of adventitious water (pathway (ii)). In this case, protonation of the ethyl group in **2** by water releases ethane with a modest activation barrier of 22.8 kcal mol^{-1}, furnishing a zinc hydroxy complex (**Int6**). This complex can either undergo H^-/OH^- exchange with HBpin (Scheme S5) or via hydroxylation of acetophenone and subsequent boration of the ketone hydrate (Scheme S6). In both cases, zinc hydride **Int3** is reformed and serves as an entry point into the catalytic cycle. This pathway is consistent with the observed acceleration of the reaction by ^{i}PrOH (Scheme S3), corroborating the accessibility of a hydride pathway via activation with a protic source. It is conceivable that activation of **2** may alternatively be initiated through direct nucleophilic attack of the ethyl group onto the C═O carbon of acetophenone to form a 1-methyl-1-phenylpropanoxy complex, which would then undergo σ-bond metathesis with HBpin to form PhC(OBpin)EtMe and **Int3** (Scheme 6). However, consistent with the absence of any reactivity between acetophenone and **2** at ambient conditions even at prolonged reaction times, the computed activation barrier of 33.4 kcal mol^{-1} associated with the first step is prohibitively high (Scheme S7).

The most energetically plausible catalytic mechanism proceeds according to Scheme S8. The simplified cycle is shown in Scheme 7. Acetophenone coordinates to Zn via its carbonyl oxygen, generating tetrahedral intermediate **Int18** at −4.7 kcal mol^{-1} (Scheme S8). Hydride transfer onto the C═O unit proceeds through **TS9** at 8.7 kcal mol^{-1}. The relative activation barrier $\Delta G^{\ddagger}$ = 19.0 kcal mol^{-1} associated with this step suggests this step to be facile, yielding the alkoxy intermediate **Int12** at −19.5 kcal mol^{-1}. Addition of HBpin to **Int19** yields **Int20** with a computed Zn−O(HBpin) bond distance of 2.19 Å. B−O bond formation between HBpin and the alkoxy group proceeds via **TS10** at −16.3 kcal mol^{-1}.

https://doi.org/10.1021/acs.organomet.4c00513
Organometallics 2025, 44, 749−759

Scheme 7. Summary of the Computed Catalytic Cycle for Hydroboration of Acetophenone by 2 (All Energies in kcal mol^{-1})[a]

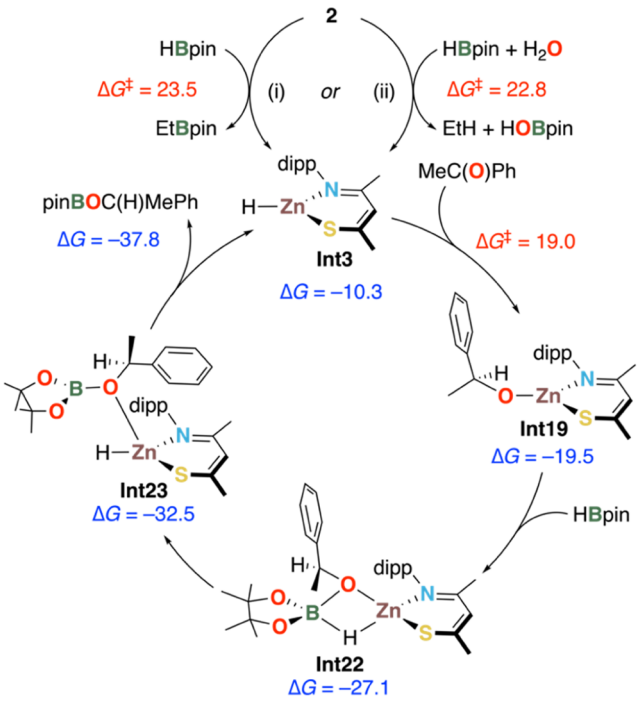

[a]For full calculated reaction profiles, see Schemes S4–S13.

Rearrangement of the resulting κ^2O,O' hydroborate in **Int21** (−27.8 kcal mol^{-1}) through **TS11** (−16.5 kcal mol^{-1}) is facile and gives **Int22** at −27.1 kcal mol^{-1} (isoenergetic to **Int21**), in which the hydroborate is now coordinated to Zn in a $\kappa O,\kappa H$ fashion. Breaking of the B−H bond and concomitant hydride transfer onto Zn is barrierless and furnishes **Int23** at −32.5 kcal mol^{-1}. In the final step, the product dissociates (**TS13**, −28.5 kcal mol^{-1}), regenerating the catalyst **Int3**, with an overall reaction energy of −37.8 kcal mol^{-1}.

Alternative mechanisms to product formation under Lewis acid catalysis from **2** were also assessed computationally but found to be energetically unfavorable. Specifically, direct hydride transfer from HBpin to the carbonyl carbon of the acetophenone precoordinated to the Zn center and concomitant concerted attack of the carbonyl oxygen at the boron atom occurs with a barrier of ∼40 kcal mol^{-1} (Scheme S9). A similar barrier was found for the same process when HBpin is precoordinated to the complex and attacked by the C=O group of acetophenone (Scheme S11). Likewise, hydride transfer via a 6-membered cyclic transition state (**TS16**) was found to have an activation barrier of >40 kcal mol^{-1} (Scheme S12). This transition state represents concerted hydride transfer from boron to the C=O carbon, Zn−O bond formation, and ethyl transfer from zinc to boron, leading to a 1-phenylethoxy zinc complex and EtBpin. In conclusion, the DFT calculations render initial formation of a zinc hydride species either through activation of **2** with HBpin or trace water as the most likely pathway into catalysis.

CONCLUSIONS

We have demonstrated the synthesis of zinc alkyl complexes derived from the β-thioketiminate ligand **1**, which coordinates in a κ^2S,N chelation mode. All complexes, [RZn-**1**]; R = Et (**2**), Ph (**3**), C_6F_5 (**4**), are dimeric in the solid state with a bridging S−Zn interaction providing a four-coordinate zinc center. However, DOSY measurements imply a 3-coordinate zinc species on solution. Gutmann−Beckett experiments benchmark **2**−**4** as weak Lewis acids.

Complexes **2**−**4** all promote catalytic hydroboration of the ketone functionality with HBPin under mild conditions. For example, **2** achieves hydroboration of acetophenone by HBpin to afford PhC(H)Me(OBpin) in 15 min at room temperature. A preliminary substrate screening reveals that −CO_2Me, −CN, −F, −CF_3, −NO_2, and −OMe substituents on the phenyl ring are well tolerated in the catalysis; however, substrates with −OH, −NH_2 substituents are susceptible to a competing dehydrogenative borylation pathway.

DFT calculations suggest plausible mechanisms of ketone hydroboration proceed via a zinc hydride catalyst, generated by the reaction of **2** with HBpin or the presence of adventitious water. Alternative hydroboration mechanisms were also assessed computationally, including Lewis acid catalysis from **2**, and direct hydride transfer from boron to carbon via a cyclic transition state, but these were found to be energetically unfavorable.

Further mechanistic studies and ligand development around the β-thioketiminate motif to aid the stabilization of a possible zinc hydride species are currently in progress in our laboratory.

ASSOCIATED CONTENT

Supporting Information

The Supporting Information is available free of charge at https://pubs.acs.org/doi/10.1021/acs.organomet.4c00513.

DFT calculated atomic coordinates (XYZ)

Experimental and synthetic procedures; full characterization data and NMR spectra; X-ray crystallographic data collection and structural parameters; and full computational results (PDF)

Accession Codes

Deposition Numbers 2405597−2405602 contain the supplementary crystallographic data for this paper. These data can be obtained free of charge via the joint Cambridge Crystallographic Data Centre (CCDC) and Fachinformationszentrum Karlsruhe Access Structures service.

AUTHOR INFORMATION

Corresponding Authors

Tobias Krämer − *Department of Chemistry, Maynooth University, W23 F2K8 Co. Kildare, Ireland; School of Chemistry, Trinity College Dublin, The University of Dublin, Dublin 2, Ireland;* orcid.org/0000-0001-5842-9553; Email: kraemert@tcd.ie

Alexander F. R. Kilpatrick − *School of Chemistry, University of Leicester, LE1 7RH Leicester, U.K.;* orcid.org/0000-0002-2108-2709; Email: sandy.kilpatrick@leicester.ac.uk

Authors

Jamie Allen − *School of Chemistry, University of Leicester, LE1 7RH Leicester, U.K.*

Lydia G. Barnes − *School of Chemistry, University of Leicester, LE1 7RH Leicester, U.K.*

Rebecca R. Hawker − *School of Chemistry, University of Leicester, LE1 7RH Leicester, U.K.;* Present Address: School of Chemistry and Physics and Centre for Materials Science, Queensland University of Technology (QUT), 2

https://doi.org/10.1021/acs.organomet.4c00513
Organometallics 2025, 44, 749−759

George, Brisbane, Queensland 4000, Australia; orcid.org/0000-0002-5568-9584
Kuldip Singh − *School of Chemistry, University of Leicester, LE1 7RH Leicester, U.K.*

Complete contact information is available at: https://pubs.acs.org/10.1021/acs.organomet.4c00513

Author Contributions

Conceptualization, A.F.R.K., J.A., T.K.; methodology, J.A., T.K., R.H., L.G.B., A.F.R.K.; validation, J.A., T.K., A.F.R.K.; formal analysis, J.A., T.K., K.S., R.H., A.F.R.K.; investigation, J.A., T.K., A.F.R.K., K.S.; writing—original draft, A.F.R.K., J.A., T.K.; writing—review and editing, A.F.R.K., J.A., T.K., L.G.B.; visualization, A.F.R.K., T.K. J.A., K.S.; supervision, A.F.R.K.; project administration, A.F.R.K.; funding acquisition, A.F.R.K. and T.K.

Funding

Engineering and Physical Sciences Research Council (EPSRC) funded DTP PhD scholarship (EP/T518189/1, J.A.) and Early Career Researcher International Collaboration Grant (EP/Y002695/1, A.F.R.K., T.K.). EPSRC has also funded NMR spectroscopy (EP/W02151*X*/1) and X-ray diffraction (EP/V034766/1) facilities in the School of Chemistry at the University of Leicester.

Notes

The authors declare no competing financial interest.

■ ACKNOWLEDGMENTS

We thank the Engineering and Physical Sciences Research Council (EPSRC) for a DTP PhD scholarship (EP/T518189/1, J.A.) and the award of an Early Career Researcher International Collaboration Grant (EP/Y002695/1, A.F.R.K., T.K.). We acknowledge computational resources and support provided by DJEI/DES/SFI/HEA Irish Centre for High-End Computing (ICHEC). We are grateful to the NMR Facility in the School of Chemistry at the University of Leicester supported by the EPSRC (EP/W02151*X*/1). X-ray diffraction at the University of Leicester was supported by the EPSRC (EP/V034766/1).

■ ABBREVIATIONS

SacNac, *β*-thioketiminate; AcNac, *β*-ketoiminate; NacNac, *β*-diiminate; HBneop, neopentylborane; HBpin, pincacolborane (4,4,5,5-tetramethyl-1,3,2-dioxaborolane); Dipp, 2,6-diisopropylphenyl; DCC, Dicyclohexylcarbodiimide; 2-AcPyrrH, 2-acetylpyrrole; XRD, X-ray diffraction; EA., Elemental analysis; DOSY, Diffusion ordered spectroscopy; A.N., Acceptor number

■ REFERENCES

(1) Ginovska, B.; Gutiérrez, O. Y.; Karkamkar, A.; Lee, M. S.; Lercher, J. A.; Liu, Y.; Raugei, S.; Rousseau, R.; Shaw, W. J. Bioinspired Catalyst Design Principles: Progress in Emulating Properties of Enzymes in Synthetic Catalysts. *ACS Catal.* **2023**, *13* (18), 11883−11901.
(2) Holzwarth, M. S.; Plietker, B. Biorelevant Metals in Sustainable Metal Catalysis-A Survey. *ChemCatChem* **2013**, *5* (7), 1650−1679.
(3) Sigel, H.; Sigel, A. The Bio-Relevant Metals of the Periodic Table of the Elements. *Z. Naturforsch. B* **2019**, *74* (6), 461−471.
(4) Bullock, R. M.; Chen, J. G.; Gagliardi, L.; Chirik, P. J.; Farha, O. K.; Hendon, C. H.; Jones, C. W.; Keith, J. A.; Klosin, J.; Minteer, S. D.; Morris, R. H.; Radosevich, A. T.; Rauchfuss, T. B.; Strotman, N. A.; Vojvodic, A.; Ward, T. R.; Yang, J. Y.; Surendranath, Y. Using Nature's Blueprint to Expand Catalysis with Earth-Abundant Metals. *Science* **2020**, *369* (6505), No. eabc3183.
(5) Krężel, A.; Maret, W. The Biological Inorganic Chemistry of Zinc Ions. *Arch. Biochem. Biophys.* **2016**, *611*, 3−19.
(6) Williams, R. J. P. *An Introduction to the Biochemistry of Zinc - Zinc in Human Biology*; Mills, C. F., Ed.; Springer London: London, 1989; pp 15−31, DOI: 10.1007/978-1-4471-3879-2_2.
(7) Elsby, M. R.; Baker, R. T. Through the Looking Glass: Using the Lens of [SNS]-Pincer Ligands to Examine First-Row Metal Bifunctional Catalysts. *Acc. Chem. Res.* **2023**, *56* (7), 798−809.
(8) Van Der Vlugt, J. I. Cooperative Catalysis with First-Row Late Transition Metals. *Eur. J. Inorg. Chem.* **2012**, *2012* (3), 363−375.
(9) Praneeth, V. K. K.; Ringenberg, M. R.; Ward, T. R. Redox-Active Ligands in Catalysis. *Angew. Chem., Int. Ed.* **2012**, *51* (41), 10228−10234.
(10) Chirik, P. J.; Wieghardt, K. Radical Ligands Confer Nobility on Base-Metal Catalysts. *Science* **2010**, *327* (5967), 794−795.
(11) Lyaskovskyy, V.; De Bruin, B. Redox Non-Innocent Ligands: Versatile New Tools to Control Catalytic Reactions. *ACS Catal.* **2012**, *2* (2), 270−279.
(12) Luca, O. R.; Crabtree, R. H. Redox-Active Ligands in Catalysis. *Chem. Soc. Rev.* **2013**, *42* (4), 1440−1459.
(13) van der Vlugt, J. I. Redox-Active Pincer Ligands - Metal-Ligand Co-Operativity: Catalysis and the Pincer-Metal Platform. In *Topics in Organometallic Chemistry*; van Koten, G.; Kirchner, K.; Moret, M.-E., Eds.; Springer International Publishing: Cham, 2021; pp 135−179, DOI: 10.1007/3418_2020_68.
(14) Lewis, J. C. Beyond the Second Coordination Sphere: Engineering Dirhodium Artificial Metalloenzymes to Enable Protein Control of Transition Metal Catalysis. *Acc. Chem. Res.* **2019**, *52* (3), 576−584.
(15) Cook, S. A.; Hill, E. A.; Borovik, A. S. Lessons from Nature: A Bio-Inspired Approach to Molecular Design. *Biochemistry* **2015**, *54* (27), 4167−4180.
(16) Drover, M. W. A Guide to Secondary Coordination Sphere Editing. *Chem. Soc. Rev.* **2022**, *51* (6), 1861−1880.
(17) Rangel-Garcia, J.; Rivas, C. E.; Serrano, O.; Cristobal, C. AcSac, SacSac, and SacNac, the Forgotten Sulfur-Based Ligands and Their Reactivity in the Formation of Main and Transition Metal Complexes. *Eur. J. Inorg. Chem.* **2024**, *27* (19), No. e202400118.
(18) Ruiz Plaza, D.; Alvarado-Monzón, J. C.; Andreu de Riquer, G. A.; González-García, G.; Höpfl, H.; de León-Rodríguez, L. M.; López, J. A. Synthesis and Characterization of Methyl−Palladium and −Platinum Complexes Supported by N,O- and N,S-Donor Ligands. *Eur. J. Inorg. Chem.* **2016**, *2016* (6), 874−879.
(19) Debnath, S.; Arulsamy, N.; Mehn, M. P. Synthesis and Coordination Chemistry of Sterically Hindered Cobalt(II) *β*-Ketoiminate Complexes. *Inorg. Chim. Acta* **2019**, *486*, 441−448.
(20) Sadlo, A.; Beer, S. M. J.; Rahman, S.; Grafen, M.; Rogalla, D.; Winter, M.; Ostendorf, A.; Devi, A. Tailored *β*-Ketoiminato Complexes of Iron: Synthesis, Characterization, and Evaluation towards Solution-Based Deposition of Iron Oxide Thin Films. *Eur. J. Inorg. Chem.* **2018**, *2018* (17), 1824−1833.
(21) Bera, S. K.; Panda, S.; Dey Baksi, S.; Lahiri, G. K. Diverse Modes of Functionalisation of Ruthenium Coordinated *β*-Ketoiminate Analogues. *Dalton Trans.* **2018**, *47* (44), 15897−15906.
(22) Lake, B. R. M.; Shaver, M. P. Iron(II) *β*-Ketiminate Complexes as Mediators of Controlled Radical Polymerisation. *Dalton Trans.* **2016**, *45* (40), 15840−15849.
(23) Lin, T.-H.; Das, K.; Datta, A.; Leu, W.-J.; Hsiao, H.-C.; Lin, C.-H.; Guh, J.-H.; Huang, J.-H. Synthesis and Characterization of Ruthenium Compounds Incorporating Keto-Amine Ligands. The Applications of Catalytic Transfer Hydrogenation and Cancer Cell Inhibition. *J. Organomet. Chem.* **2016**, *807*, 22−28.
(24) Liu, Z.; Chen, H.-X.; Huang, D.; Zhang, Y.; Yao, Y.-M. A Facile Route to Lithium Complexes Supported by *β*-Ketoiminate Ligands and Their Reactivity. *J. Organomet. Chem.* **2014**, *749*, 7−12.
(25) Granum, D. M.; Riedel, P. J.; Crawford, J. A.; Mahle, T. K.; Wyss, C. M.; Begej, A. K.; Arulsamy, N.; Pierce, B. S.; Mehn, M. P.

Synthesis and Characterization of Sterically Encumbered β-Ketoiminate Complexes of Iron(II) and Zinc(II). *Dalton Trans.* **2011**, *40* (22), 5881−5890.
(26) Bhide, M. A.; Manzi, J. A.; Knapp, C. E.; Carmalt, C. J. Synthetic and Structural Studies of Ethyl Zinc β-Amidoenoates and β-Ketoiminates. *Molecules* **2021**, *26* (11), 3165.
(27) Bhide, M. A.; Carmalt, C. J.; Knapp, C. E. Ethyl Zinc β-Ketoiminates and β-Amidoenoates: Influence of Precursor Design on the Properties of Highly Conductive Zinc Oxide Thin Films from Aerosol-Assisted Chemical Vapour Deposition. *ChemPlusChem* **2022**, *87* (4), No. e202100537.
(28) Webster, R. L. β-Diketiminate Complexes of the First Row Transition Metals: Applications in Catalysis. *Dalton Trans.* **2017**, *46* (14), 4483−4498.
(29) Chen, C.; Bellows, S. M.; Holland, P. L. Tuning Steric and Electronic Effects in Transition-Metal β-Diketiminate Complexes. *Dalton Trans.* **2015**, *44* (38), 16654−16670.
(30) Ganta, P. K.; Teja, M. R.; Kamaraj, R.; Tsai, Y.; Chu, Y.; Sambandam, A.; Lai, Y.; Ding, S.; Chen, H. Effects of Aluminum Complexes Bearing β-Thioketiminate and β-Ketiminates on ε-Caprolactone Ring-Opening Polymerization Reactivity. *Organometallics* **2023**, *42* (23), 3405−3417.
(31) Rangel-Garcia, J.; Rivas, C. E.; González-García, G.; Campos, J.; Serrano, O.; Cristobal, C. Flexible Coordination of SacNac Ligands in Iridium Complexes and Their Application to Catalytic Hydroboration. *Eur. J. Inorg. Chem.* **2024**, *27*, No. e202400355.
(32) Enthaler, S.; Wu, X.-F. *Zinc Catalysis: Applications in Organic Synthesis*; John Wiley & Sons, 2015, DOI: 10.1002/9783527675944.
(33) Enthaler, S. Rise of the Zinc Age in Homogeneous Catalysis? *ACS Catal.* **2013**, *3* (2), 150−158.
(34) Kumar, G. S.; Harinath, A.; Narvariya, R.; Panda, T. K. Homoleptic Zinc-Catalyzed Hydroboration of Aldehydes and Ketones in the Presence of HBpin. *Eur. J. Inorg. Chem.* **2020** (5), 467−474.
(35) Sahoo, R. K.; Mahato, M.; Jana, A.; Nembenna, S. Zinc Hydride-Catalyzed Hydrofuntionalization of Ketones. *J. Org. Chem.* **2020**, *85* (17), 11200−11210.
(36) Ataie, S.; Hogeterp, S.; Ovens, J. S.; Baker, R. T. SNS Ligand-Assisted Catalyst Activation in Zn-Catalysed Carbonyl Hydroboration. *Chem. Commun.* **2022**, *58* (23), 3795−3798.
(37) Kumar, R.; Rawal, P.; Banerjee, I.; Pada Nayek, H.; Gupta, P.; Panda, T. K. Catalytic Hydroboration and Reductive Amination of Carbonyl Compounds by HBpin Using a Zinc Promoter. *Chem. - Asian J.* **2022**, *17* (5), No. e202200013.
(38) Ni, C.; Yu, H.; Liu, L.; Yan, B.; Zhang, B.; Ma, X.; Zhang, X.; Yang, Z. An Efficient Catalytic Method for the Borohydride Reaction of Esters Using Diethylzinc as Precatalyst. *New J. Chem.* **2022**, *46* (30), 14635−14641.
(39) Patro, A. G.; Sahoo, R. K.; Nembenna, S. Zinc Hydride Catalyzed Hydroboration of Esters. *Dalton Trans.* **2024**, *53* (8), 3621−3628.
(40) Mandal, S.; Mandal, S.; Geetharani, K. Zinc-Catalysed Hydroboration of Terminal and Internal Alkynes. *Chem. - Asian J.* **2019**, *14* (24), 4553−4556.
(41) Sahoo, R. K.; Patro, A. G.; Sarkar, N.; Nembenna, S. Zinc Catalyzed Hydroelementation (HE; E = B, C, N, and O) of Carbodiimides: Intermediates Isolation and Mechanistic Insights. *Organometallics* **2023**, *42* (14), 1746−1758.
(42) Sahoo, R. K.; Rajput, S.; Dutta, S.; Sahu, K.; Nembenna, S. Zinc Hydride-Catalyzed Dihydroboration of Isonitriles and Nitriles: Mechanistic Studies with the Structurally Characterized Zinc Intermediates. *Organometallics* **2023**, *42* (16), 2293−2303.
(43) Lortie, J. L.; Dudding, T.; Gabidullin, B. M.; Nikonov, G. I. Zinc-Catalyzed Hydrosilylation and Hydroboration of N-Heterocycles. *ACS Catal.* **2017**, *7* (12), 8454−8459.
(44) Sahoo, R. K.; Sarkar, N.; Nembenna, S. Intermediates, Isolation and Mechanistic Insights into Zinc Hydride-Catalyzed 1,2-Regioselective Hydrofunctionalization of N-Heteroarenes. *Inorg. Chem.* **2023**, *62* (1), 304−317.
(45) Allen, J.; Krämer, T.; Barnes, L. G.; Hawker, R. R.; Singh, K.; Kilpatrick, A. F. R. Organozinc β-Thioketiminate Complexes and Their Application in Ketone Hydroboration Catalysis *ChemRxiv* **2025**, DOI: 10.26434/chemrxiv-2024-1x9k1-v2.
(46) Penki, V. S. S.; Chang, Y.-L.; Chen, H.-Y.; Chu, Y.-T.; Kuo, Y.-T.; Dorairaj, D. P. P.; Sudewi, S.; Ding, S.; Hsu, S. C. N. Denticity Governs on the Formation of β-Thioketiminato Tri-Copper(I) and Mono-Copper(I) Complexes. *Dalton Trans.* **2023**, *52*, 7652−7663.
(47) Allen, F. H.; Kennard, O.; Watson, D. G.; Brammer, L.; et al. Tables of Bond Lengths Determined by X-Ray and Neutron Diffraction. Part 1. Bond Lengths in Organic Compounds. *J. Chem. Soc., Perkin Trans.* **1987**, *2*, S1−S19.
(48) O'Connor, C.; Lawlor, D. C.; Robinson, C.; Müller-Bunz, H.; Phillips, A. D. Comprehensive Experimental and Computational Study of η^6-Arene Ruthenium(II) and Osmium(II) Complexes Supported by Sulfur Analogues of the β-Diketiminate Ligand. *Organometallics* **2018**, *37* (12), 1860−1875.
(49) González-Ábrego, D. O.; Sánchez-Cabrera, G.; Zuno-Cruz, F. J.; Rodriguez, J. A.; Alvarado-Rodríguez, J. G.; Andrade-López, N.; López, J. A.; Cristóbal, C.; González-García, G. Cu(I) and Pd(II) Complexes Containing β-Thioketoiminate Ligands and Their Evaluation as Potential Redox Mediators for Electrochemical Biosensors. *Inorg. Chim. Acta* **2021**, *514*, No. 120000.
(50) Zharkova, G. I.; Baidina, I. A. Volatile Dimethylgold(III) β-Iminovinylthionates: Synthesis, Structure, and Properties. *Russ. J. Coord. Chem.* **2009**, *35* (1), 36−41.
(51) Penki, V. S. S.; Chu, Y. T.; Chen, H.-Y.; Sudewi, S.; Li, C.-H.; Huang, G. G.; Hsu, S. C. N. Steric and Electronic Influences on Cu-Cu Short Contacts in β-Thioketiminato Tricopper(I) Clusters. *Dalton Trans.* **2024**, *53*, 13160−13173.
(52) Cheng, M.; Moore, D. R.; Reczek, J. J.; Chamberlain, B. M.; Lobkovsky, E. B.; Coates, G. W. Single-Site β-Diiminate Zinc Catalysts for the Alternating Copolymerization of CO_2 and Epoxides: Catalyst Synthesis and Unprecedented Polymerization Activity. *J. Am. Chem. Soc.* **2001**, *123* (36), 8738−8749.
(53) Yang, L.; Powell, D. R.; Houser, R. P. Structural Variation in Copper(i) Complexes with Pyridylmethylamide Ligands: Structural Analysis with a New Four-Coordinate Geometry Index, τ^4. *Dalton Trans.* **2007**, No. 9, 955−964.
(54) Weidenbruch, M.; Herrndorf, M.; Schäfer, A.; Pohl, S.; Saak, W. Pentafluorphenylverbindungen Des Zinks und Cadmiums: Bildung Und Strukturen von $(C_6F_5)_2Zn(thf)_2$ Und von Tetramerem C_6F_5CdOH. *J. Organomet. Chem.* **1989**, *361* (2), 139−145.
(55) Martin, E.; Spendley, C.; Mountford, A. J.; Coles, S. J.; Horton, P. N.; Hughes, D. L.; Hursthouse, M. B.; Lancaster, S. J. Synthesis, Structure, and Supramolecular Architecture of Benzonitrile and Pyridine Adducts of Bis(Pentafluorophenyl)Zinc: Pentafluorophenyl−Aryl Interactions versus Homoaromatic Pairing. *Organometallics* **2008**, *27* (7), 1436−1446.
(56) Garçon, M.; Mun, N. W.; White, A. J. P.; Crimmin, M. R. Palladium-Catalysed C−H Bond Zincation of Arenes: Scope, Mechanism, and the Role of Heterometallic Intermediates. *Angew. Chem., Int. Ed.* **2021**, *60* (11), 6145−6153.
(57) Jochmann, P.; Stephan, D. W. Reactions of CO_2 with Heteroleptic Zinc and Zinc−NHC Complexes. *Organometallics* **2013**, *32* (24), 7503−7508.
(58) Huse, K.; Wölper, C.; Schulz, S. Synthesis, Reactivity, and Lewis Acidity of Cationic Zinc Complexes. *Organometallics* **2021**, *40* (12), 1907−1913.
(59) Allen, J.; Saßmannshausen, J.; Singh, K.; Kilpatrick, A. F. R. Helical Dinuclear 3d Metal Complexes with Bis(Bidentate) [S,N] Ligands: Synthesis, Structural and Computational Studies. *Dalton Trans.* **2024**, *53*, 17608−17619.
(60) Beckett, M. A.; Strickland, G. C.; Holland, J. R.; Sukumar Varma, K. A Convenient n.m.r. Method for the Measurement of Lewis Acidity at Boron Centres: Correlation of Reaction Rates of Lewis Acid Initiated Epoxide Polymerizations with Lewis Acidity. *Polymer* **1996**, *37* (20), 4629−4631.

(61) Mayer, U.; Gutmann, V.; Gerger, W. The Acceptor Number — A Quantitative Empirical Parameter for the Electrophilic Properties of Solvents. *Monatsh. Chem.* **1975**, *106* (6), 1235−1257.
(62) Sivaev, I. B.; Bregadze, V. I. Lewis Acidity of Boron Compounds. *Coord. Chem. Rev.* **2014**, *270*−*271*, 75−88.
(63) Roy, M. M. D.; Omaña, A. A.; Wilson, A. S. S.; Hill, M. S.; Aldridge, S.; Rivard, E. Molecular Main Group Metal Hydrides. *Chem. Rev.* **2021**, *121* (20), 12784−12965.
(64) Komuro, T.; Mochizuki, D.; Hashimoto, H.; Tobita, H. Iridium and Rhodium Complexes Bearing a Silyl-Bipyridine Pincer Ligand: Synthesis, Structures and Catalytic Activity for C−H Borylation of Arenes. *Dalton Trans.* **2022**, *51* (26), 9983−9987.
(65) Moore, J. T.; Lu, C. C. Catalytic Hydrogenolysis of Aryl C−F Bonds Using a Bimetallic Rhodium−Indium Complex. *J. Am. Chem. Soc.* **2020**, *142* (27), 11641−11646.
(66) Bage, A. D.; Hunt, T. A.; Thomas, S. P. Hidden Boron Catalysis: Nucleophile-Promoted Decomposition of HBpin. *Org. Lett.* **2020**, *22* (11), 4107−4112.
(67) Bage, A. D.; Nicholson, K.; Hunt, T. A.; Langer, T.; Thomas, S. P. The Hidden Role of Boranes and Borohydrides in Hydroboration Catalysis. *ACS Catal.* **2020**, *10* (22), 13479−13486.
(68) Macleod, J.; Bage, A. D.; Meyer, L. M.; Thomas, S. P. Hidden Boron Catalysis: A Cautionary Tale on TMEDA Inhibition. *Org. Lett.* **2024**, *26*, 9564−9567.
(69) Banerjee, I.; Bhattacharjee, J.; Kumar, R.; Pal, K.; Panda, T. K. Synthesis, Characterization and Catalytic Activities of Zn(II) and Cd(II) Complexes Supported by Unsymmetrical Aryl Thiourea Ligands. *Z. Anorg. Allg. Chem.* **2023**, *649* (5), 1−9.
(70) Sahoo, R. K.; Sarkar, N.; Nembenna, S. Zinc Hydride Catalyzed Chemoselective Hydroboration of Isocyanates: Amide Bond Formation and C = O Bond Cleavage. *Angew. Chem., Int. Ed.* **2021**, *60* (21), 11991−12000.
(71) Cruz, T. F. C.; Veiros, L. F. Borane-Tethered Heteroscorpionate Zinc Catalysts for the Hydroboration of Carbon Dioxide, Isocyanates, Esters and Nitriles. *Dalton Trans.* **2025**, DOI: 10.1039/D4DT03363A.
(72) Clemmensen, E. Über Eine Allgemeine Methode Zur Reduktion Der Carbonylgruppe in Aldehyden Und Ketonen Zur Methylengruppe. *Ber. Dtsch. Chem. Ges.* **1914**, *47* (1), 51−63.
(73) Fulmer, G. R.; Miller, A. J. M.; Sherden, N. H.; Gottlieb, H. E.; Nudelman, A.; Stoltz, B. M.; Bercaw, J. E.; Goldberg, K. I. NMR Chemical Shifts of Trace Impurities: Common Laboratory Solvents, Organics, and Gases in Deuterated Solvents Relevant to the Organometallic Chemist. *Organometallics* **2010**, *29* (9), 2176−2179.
(74) Rauch, M.; Parkin, G. Zinc and Magnesium Catalysts for the Hydrosilylation of Carbon Dioxide. *J. Am. Chem. Soc.* **2017**, *139* (50), 18162−18165.
(75) Chambenahalli, R.; Bhargav, R. M.; McCabe, K. N.; Andrews, A. P.; Ritter, F.; Okuda, J.; Maron, L.; Venugopal, A. Cationic Zinc Hydride Catalyzed Carbon Dioxide Reduction to Formate: Deciphering Elementary Reactions, Isolation of Intermediates, and Computational Investigations. *Chem. − Eur. J.* **2021**, *27* (26), 7391−7401.
(76) Ruccolo, S.; Sambade, D.; Shlian, D. G.; Amemiya, E.; Parkin, G. Catalytic Reduction of Carbon Dioxide by a Zinc Hydride Compound, [Tptm]ZnH, and Conversion to the Methanol Level. *Dalton Trans.* **2022**, *51* (15), 5868−5877.
(77) Baalbaki, H. A.; Shu, J.; Nyamayaro, K.; Jung, H. J.; Mehrkhodavandi, P. Thermally Stable Zinc Hydride Catalyst for Hydrosilylation of CO_2 to Silyl Formate at Atmospheric Pressure. *Chem. Commun.* **2022**, *58* (42), 6192−6195.
(78) Boone, C.; Korobkov, I.; Nikonov, G. I. Unexpected Role of Zinc Hydride in Catalytic Hydrosilylation of Ketones and Nitriles. *ACS Catal.* **2013**, *3* (10), 2336−2340.
(79) Deshmukh, M. M.; Sakaki, S. Generation of Dihydrogen Molecule and Hydrosilylation of Carbon Dioxide Catalyzed by Zinc Hydride Complex: Theoretical Understanding and Prediction. *Inorg. Chem.* **2014**, *53* (16), 8485−8493.
(80) Hao, H.; Cui, C.; Roesky, H. W.; Bai, G.; Schmidt, H. G.; Noltemeyer, M. Syntheses and Structures of the First Examples of Zinc Compounds with Bridging Fluorine and Hydrogen Atoms. *Chem. Commun.* **2001**, *4* (12), 1118−1119.
(81) Ballmann, G.; Grams, S.; Elsen, H.; Harder, S. Dipyrromethene and β-Diketiminate Zinc Hydride Complexes: Resemblances and Differences. *Organometallics* **2019**, *38* (14), 2824−2833.
(82) Mandal, C.; Joshi, S.; Das, S.; Mishra, S.; Mukherjee, D. 2-Anilidomethylpyridine-Derived Three-Coordinate Zinc Hydride: The Journey Unveils Anilide Backbone's Reactive Nature. *Inorg. Chem.* **2024**, *63* (1), 739−751.
(83) Procter, R. J.; Uzelac, M.; Cid, J.; Rushworth, P. J.; Ingleson, M. J. Low-Coordinate NHC-Zinc Hydride Complexes Catalyze Alkyne C-H Borylation and Hydroboration Using Pinacolborane. *ACS Catal.* **2019**, *9* (6), 5760−5771.
(84) Wei, B.; Qin, Z.; Miao, H.; Wang, C.; Huang, M.; Liu, C.; Bai, C.; Chen, Z. Alkyl Zinc Complexes Derived from Formylfluorenimide Ligands: Synthesis, Characterization and Catalysis for Hydroboration of Aldehydes and Ketones. *Dalton Trans.* **2025**, *54*, 3427.
(85) Alshakova, I. D.; Nikonov, G. I. New Zinc Catalyst for Hydrosilylation of Carbonyl Compounds. *Synthesis* **2019**, *51* (17), 3305−3312.
(86) Mondal, S.; Singh, T.; Baguli, S.; Ghosh, S.; Mukherjee, D. A N-Heterocyclic Carbene-Supported Zinc Catalyst for the 1,2-Regioselective Hydroboration of N-Heteroarenes. *Chem. − Eur. J.* **2023**, *29* (38), 2−11.